Applied Physics Letters

Improved nucleation of AlN on *in situ* nitrogen doped graphene for GaN quasi-van der Waals epitaxy

Cite as: Appl. Phys. Lett. **117**, 051601 (2020); https://doi.org/10.1063/5.0016054
Submitted: 01 June 2020 . Accepted: 22 July 2020 . Published Online: 03 August 2020

Yang Chen, Hang Zang, Ke Jiang, Jianwei Ben, Shanli Zhang, Zhiming Shi, Yuping Jia, Wei Lü, Xiaojuan Sun, and Dabing Li

Applied Physics Letters ARTICLE scitation.org/journal/apl

Improved nucleation of AlN on *in situ* nitrogen doped graphene for GaN quasi-van der Waals epitaxy

Cite as: Appl. Phys. Lett. **117**, 051601 (2020); doi: 10.1063/5.0016054
Submitted: 1 June 2020 · Accepted: 22 July 2020 ·
Published Online: 3 August 2020

Yang Chen,[1,2] Hang Zang,[1,2] Ke Jiang,[1,2] Jianwei Ben,[1,3] Shanli Zhang,[1,2] Zhiming Shi,[1,2] Yuping Jia,[1,2] Wei Lü,[1,4] Xiaojuan Sun,[1,2,a)] and Dabing Li[1,2,b)]

AFFILIATIONS

[1]State Key Laboratory of Luminescence and Applications, Changchun Institute of Optics, Fine Mechanics and Physics, Chinese Academy of Sciences, Changchun 130033, China
[2]Center of Materials Science and Optoelectronics Engineering, University of Chinese Academy of Sciences, Beijing 100049, China
[3]College of Materials Science and Engineering, Shenzhen University, Shenzhen 518071, China
[4]Key Laboratory of Advanced Structural Materials, Ministry of Education, Changchun University of Technology, Changchun 130012, China

[a)]Author to whom correspondence should be addressed: sunxj@ciomp.ac.cn
[b)]Electronic mail: lidb@ciomp.ac.cn

ABSTRACT

In the present work, improved crystal quality of GaN on a graphene-covered sapphire substrate was achieved compared to GaN grown on a bare sapphire substrate, and the growth mechanism of GaN quasi-van der Waals epitaxy with an AlN nucleation layer was clarified using metal-organic chemical vapor deposition. The *in situ* N-doping of graphene by an NH_3 source during AlN growth was responsible for AlN nucleation. The first-principles calculation indicated that N atoms doped initially at the step edges of graphene and subsequently at its center and AlN nuclei followed the same sequence, which is consistent with experimental observations of nucleation. The lower migration barrier of Al atoms (0.07 eV) on graphene created larger AlN nuclei compared to that on bare sapphire (0.21 eV), leading to improved quality of the upper GaN epilayer with lower defect density. This work offers guidance for precisely controlling the nucleation morphology and density of GaN base materials and thus realizing high-quality epitaxial materials and related high-performance devices by quasi-van der Waals epitaxy.

GaN is a wide bandgap semiconductor with many useful properties, such as a 3.4 eV direct bandgap, excellent thermal and chemical stabilities, a high break voltage, and a large electron saturation velocity.[1–5] All these have made it a promising material for use in light-emitting diodes, lasers, photodetectors, and high voltage power and electronic devices.[6–11] Because of the lack of a suitable substrate, GaN is generally acquired by heteroepitaxy. The intrinsic lattice and thermal mismatch between GaN and the substrate induce stress and defects even though the growth method has been optimized.[12,13] An even more efficient growth strategy is needed to further improve the quality of GaN for enhancing device performance. Recently, the potential of van der Waals epitaxy of III-nitrides based on two dimensional graphene for both improving material quality and being potentially used in flexible and wearable electronic devices was reported.[14–17] The sp^2 bonded graphene, which is hexagonal in structure, has excellent thermal and chemical stabilities and weakly bonded layers.[18–20] Given the corresponding weak van der Waals interaction between the GaN epilayer and graphene, graphene may act as a buffer for GaN growth to solve the aforementioned problems with heteroepitaxy. Thanks to the weak van der Waals force, the III-nitride epilayer could be easily transferred from rigid epitaxial substrates (such as sapphire) onto other flexible substrates (such as plastic) by simple mechanical exfoliation, and potential III-nitride applications in flexible or wearable devices could be achieved.[16,17]

One of the obstacles to graphene-based GaN van der Waals epitaxy is the difficulty of nucleating GaN on a perfect graphene surface because of the lack of dangling bonds and bonding electrons. Compared to GaN, AlN is easier to nucleate on graphene because of its higher viscosity, which makes it an ideal interlayer for preparing a high-quality GaN epilayer.[21,22] In addition, N_2/O_2 plasma can induce

N/O atom doping in the graphene lattice and the formation of C–N/C–O bonding configurations, which act as nucleation sites for III-nitrides.[23–25] The defects and wrinkles induced during graphene growth or transfer can also serve as natural nucleation sites.[26–28] Considering the covalent bonding between III-nitrides and defects or doped atoms underneath graphene during nucleation, it is better to define the growth of III-nitrides on graphene as a quasi-van der Waals process. In spite of the effort dedicated to investigating graphene-based quasi-van der Waals epitaxy of GaN and other III-nitrides, the associated growth mechanism remains to be clarified. Further effort should be made to reveal the nucleation and growth mechanism of quasi-van der Waals epitaxy, thus precisely controlling the growth morphology and crystal quality of the epitaxial materials.

Here, we investigated the evolution of quasi-van der Waals epitaxy of AlN nucleation and the GaN film on graphene by metal-organic chemical vapor deposition (MOCVD). The corresponding growth mechanism was clarified based on both experiments and the first-principles calculation. We found that *in situ* N-doping of graphene by an NH_3 source during AlN growth controls AlN nucleation from the edge of graphene to the center. The low migration barrier of Al atoms (0.07 eV) induced larger AlN nuclei on graphene and subsequent growth of GaN with a lower dislocation density. The present work provides guidance for precisely controlling the growth morphology and crystal quality of GaN epitaxial materials on graphene.

The detailed graphene transfer and GaN epitaxy processes with an AlN nucleation layer by MOCVD are described in Fig. S1, supplementary material. Trimethylaluminum (TMAl), trimethylgallium (TMGa), and NH_3 were used as sources of Al, Ga, and N during the MOCVD growth. The GaN film grown on graphene and sapphire was called g-GaN and s-GaN, respectively. We used growth interruptions to illustrate the evolution of morphology; corresponding images from a scanning electron microscope (SEM; S4800, Hitachi) are shown in Fig. 1. AlN nuclei were not observed in the first 20 s on the bare sapphire substrate, as shown in Fig. 1(a). The sapphire substrate possesses a spatially uniform surface and a relatively higher migration barrier for Al atoms; thus, the vapor supersaturation as well as background thermal energy must be high enough to induce Al atom migration and nucleus formation.[29] At 2 min, AlN nuclei with a small size and high density were uniformly distributed on the sapphire substrate; the nuclei continued to grow to 6 min, as shown in Figs. 1(b) and 1(c). This is mainly attributed to the fact that the accumulated background thermal energy exceeded the migration barrier, and Al atoms began migrating and then encountered to one another, forming AlN nuclei. AlN nuclei exhibited markedly different growth behaviors on the graphene-covered sapphire substrate, as shown in Figs. 1(f)–1(h). Initially, AlN nuclei were visible at specific positions on graphene, as shown in Fig. 1(f). Comparisons of the morphology between pristine graphene and 20 s AlN growth in the large-view field are shown in Figs. S2(a) and S2(b), supplementary material. Wrinkles and broken boundaries were observed on pristine graphene, and AlN nuclei at these positions had similar shapes, sizes, and density compared to the wrinkles and boundaries in graphene. We speculate that AlN initially nucleated at the wrinkles and boundaries of graphene with selective nucleation growth. Over time, the AlN nuclei spread away from the wrinkles and boundaries and then converged on one another on the center of graphene, which is further expressed in the large-view field of SEM in Figs. S2(b)–S2(d), supplementary material. Unlike the uniform surface of sapphire, the inherent defects and doped atoms in graphene provide sites of relatively easy attachment for Al adatoms; thus, surface migration may be directionally biased to these positions. This process is known as non-uniform nucleation growth. In this way, Al adatoms with a migration distance larger than the defects or dopant spacing tend to converge at these sites, forming larger AlN nuclei than those formed by uniform nucleation on sapphire.[30] Also, the larger grain size of AlN nuclei on graphene had a parasitical structure relationship with subsequent GaN growth, inducing different growth of GaN, as shown in Figs. 1(d) and 1(i). The larger size of AlN nuclei on graphene would lead to less boundaries of the up-grown GaN, which is beneficial for the reduction of threading dislocations (TDs). The full-coverage GaN film was achieved after 1 h of growth, as shown in Figs. 1(e) and 1(j); the thickness, measured by Filmetrics, was around 3 μm (Fig. S3, supplementary material). Note that s-GaN exhibited visible pinholes on its surface, which might have belonged to TDs in the GaN epilayer. However, these pinholes were absent in g-GaN.

To reveal the growth mechanism of graphene-assisted quasi-van der Waals epitaxy of GaN with an AlN nucleation layer, we studied

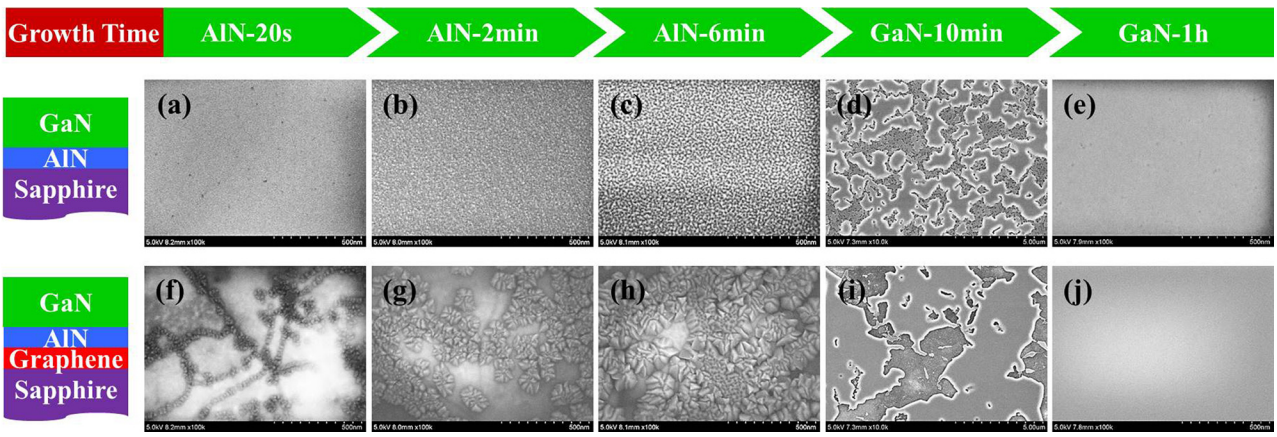

FIG. 1. (a)–(c) SEM images of AlN interrupted nucleation on sapphire and (f)–(h) graphene with nucleation times of 20 s, 2 min, and 6 min, respectively. (d) and (i) GaN epitaxy on the AlN nucleation layer after 10 min and (e) and (j) 1 h.

the properties of graphene by SEM, atomic force microscopy (AFM; MultiMode 8, Bruker), and Raman spectroscopy (LabRAM HR Evolution, Horiba), as shown in Fig. 2. A digital photograph of graphene on a 2 in. sapphire substrate is shown in Fig. 2(a), and the corresponding SEM image is shown in Fig. 2(b). Wrinkles marked by yellow dashed lines, existed on graphene and a few broken boundaries, circled by red dashed lines, formed where the wrinkles overlapped. Both the graphene wrinkles and boundaries belonged to step edges, and these edge defects were mainly induced during thermal release due to the mismatch in the thermal expansion coefficient between graphene and sapphire.[31] The morphology of graphene measured by AFM, in Fig. 2(c), was consistent with the SEM results, and the corresponding height profile showed an average height of 3 nm for graphene wrinkles. Figure 2(e) shows Raman spectra of pristine graphene as well as graphene after AlN growth for 20 s and 2 min and 6 min. The characteristic D, G, and 2D bands of pristine graphene were located at 1345, 1585, and 2696 cm^{-1}, respectively. The intensity ratio of I_{2D}/I_G was around 3.6, highlighting the monolayer nature of as-transferred pristine graphene.[32] The graphene defect density was positively related to the D band intensity, and the asymmetry of N heteroatoms in the graphene lattice induced charge transfer, which is evident by the G band shift.[33,34] We summarized the data on I_D/I_G and variation in the G band position in Fig. 2(f). During AlN growth in the MOCVD system, graphene was treated with continuous H_2 and NH_3 at a relatively high temperature (930 °C). Because of the etching effects of H_2 on graphene, especially at high temperatures, I_D/I_G exhibited an increasing trend (0.22–0.5), which implies an increased defect density in graphene. At the same time, the G band of graphene gradually shifted to a high wavenumber (1585–1598 cm^{-1}) from 20 s to 6 min, which was attributed to the fact that *in situ* N-doping in graphene created unusual carriers that interact with lattice vibrations.[35] These results indicated that N atoms decomposed from NH_3 can induce *in situ* N-doping in graphene and form C–N bonds. Further evidence of C–N bonds in graphene was provided by N1s x-ray photoelectron spectroscopy (XPS; VG ESCALAB MKII, Thermo Scientific), as shown in Fig. S3, supplementary material. Sp^2 C–N (398.7 eV) and sp^3 C–N bonds (399.8 eV) were deconvoluted from N1s core-level spectra, which implied the presence of two types of C–N bonds in graphene. The existence of C–N bonds on the surface of graphene changed the bonding environment of Al atoms during the epitaxy process, and thus, it can be deduced that the C–N bonds provided the new site for AlN nucleation.

The microstructural properties of g-GaN were investigated by transmission electron microscopy (TEM; Tecnai G2 F20 S-TWIN, FEI), as shown in Fig. 3(a). Graphene with an overlapping layered structure of about 3 nm was sandwiched between sapphire and the AlN nucleation layer even after high-temperature growth. The greater thickness of the graphene layer in TEM observations was due to the existence of wrinkles, and the result was consistent with the

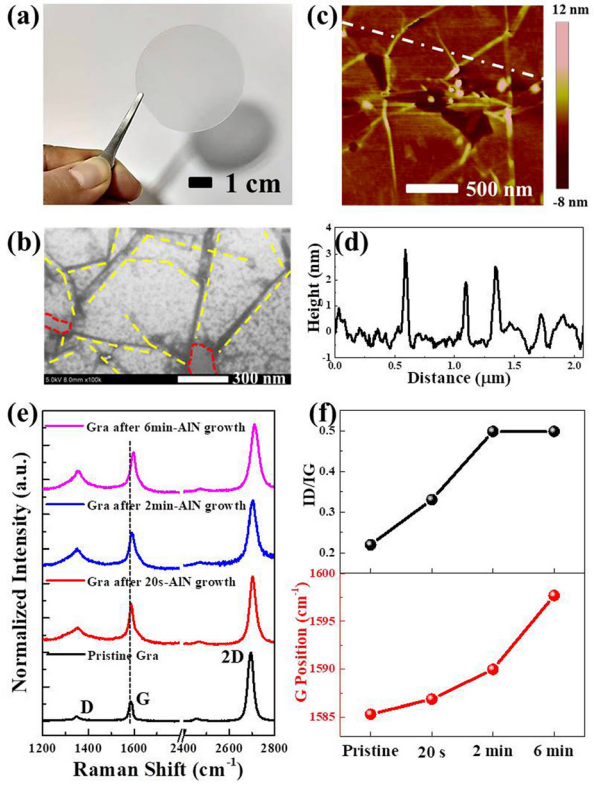

FIG. 2. (a) Photograph of graphene transferred onto 2 in. sapphire. (b) SEM and (c) AFM images of as-transferred graphene on sapphire. (d) Surface height profile distribution of graphene extracted from AFM data. (e) Raman spectra and (f) related variation of graphene after gradual AlN growth.

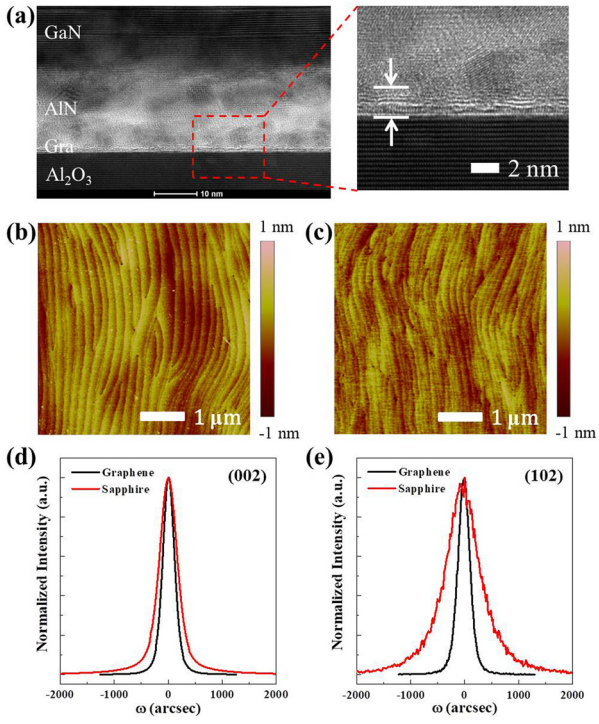

FIG. 3. (a) The cross-sectional TEM image of GaN films grown on graphene/sapphire substrates. (b) AFM images of GaN films grown on graphene and (c) sapphire. (d) FWHM of XRD rocking curves of (002) and (e) (102) GaN films grown on graphene and sapphire.

AFM-measured height in Fig. 2(d). The morphologies of g-GaN and s-GaN were measured by AFM, and the results are shown in Figs. 3(b) and 3(c), respectively. Atomic steps on the GaN surface were obvious in both samples; g-GaN exhibited wider and more regular atomic steps than s-GaN, which might be because the initial islands of g-GaN were larger and less dense; see Fig. 1(i). Although the root mean square roughness (Rq) of g-GaN (0.244 nm) was slightly higher than that of s-GaN (0.202 nm), there were fewer visible TDs on the surface of g-GaN ($1.16 \times 10^8\,cm^{-2}$) than s-GaN ($3.12 \times 10^8\,cm^{-2}$). The (002) and (102) GaN x-ray diffraction (XRD; D8 Discover, Bruker) rocking curves were measured using a Ge (220) bicrystal monochromator, as shown in Figs. 3(d) and 3(e), and the full width at half maximum (FWHM) was related to the screw dislocation and edge dislocation density. The off-axis reflection was measured by a skew-symmetric geometry. The (002) and (102) FWHM of the XRD rocking curves were 251 and 265 arc sec for g-GaN, both of which exhibited a distinct decline, compared to 421 and 738 arc sec for s-GaN, respectively. In addition, g-GaN had stronger near-band edge emission at 362 nm compared to s-GaN, and no significant defect-related emission peak was observed, as shown in Fig. S5, supplementary material. These results are consistent with the reduced TD density obtained from the AFM images, which implies better crystal quality of GaN epitaxy on graphene.

The first-principles calculation was performed to reveal the physical mechanism behind the AlN nucleation and reduction in the GaN dislocation on graphene. This method was based on density functional theory with the projector augmented wave (PAW) method implemented in the Vienna *ab initio* simulation package (VASP).[36] The structure formation energy of N-doped graphene (black polyline) and Al absorption energy on these structures (red polyline) were calculated, as shown in Fig. 4(a), to reveal the nucleation mechanism of AlN on N-doping in graphene. The absorption energies of Al atoms at various C–N bonding sites were below −0.41 eV, which implies that AlN nuclei preferred to nucleate over these sites. Therefore, *in situ* N-doping of graphene by NH_3 in MOCVD can provide high density nucleation sites for AlN growth. In addition, the structure formation energy of two types of N-dopants at graphene step edges (structures 1–4) and centers (structures 5 and 6) was calculated; the markedly lower formation energy at graphene edges indicated that C–N bonding was easier at step edges (below −1.22 eV) of graphene rather than its centers (above 3.42 eV). The step edges (wrinkles and boundaries) in graphene possess more defects and dangling bonds, which provide lone pair electrons for C–N bonding and lead to easier C–N bond formation in the experimental condition. To assess the mobility of Al atoms on different substrates, we used a climbing image nudged elastic band (CI-NEB) method to locate the transition states of Al atom migration on graphene and sapphire; three images were created to connect the initial and final configurations.[37] As shown in Figs. 4(b) and 4(c), the calculated Al migration barrier was lower on defect-free graphene (0.07 eV) than on bare sapphire (0.21 eV), which is consistent with the weak van der Waals interaction between Al atoms and graphene. Detailed theoretical methods of the first-principles calculation are described in the supplementary material.

The growth model of GaN quasi-van der Waals epitaxy with AlN nuclei on graphene is proposed in Figs. 4(d)–4(g). At the beginning stage, in Fig. 4(d), the *in situ* C–N bonds form at the step edges (wrinkles and broken boundaries) of graphene because of the low formation

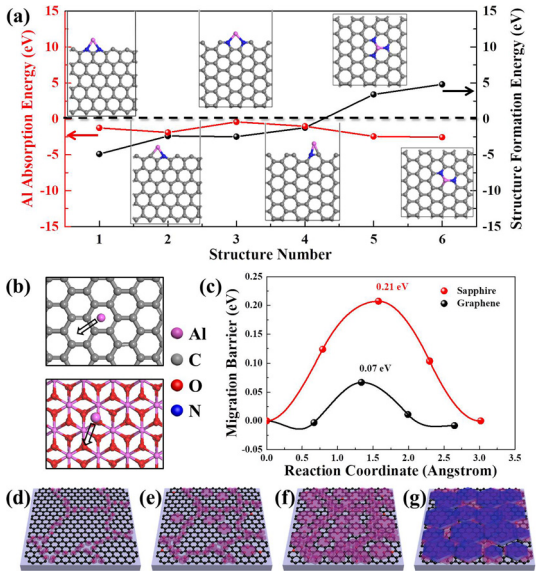

FIG. 4. (a) First-principles calculation of graphene structure formation energy by N-dopant and Al atom absorption energy among these structures. (b) Schematic diagrams of Al atom migration on graphene and sapphire and (b) the calculated migration barrier. (d)–(g) Schematic diagrams of AlN and GaN growth on graphene.

energy and serve as nucleation sites for AlN. Over time, greater reactive activation among N atoms, H_2, and graphene triggers N-doping at the centers of graphene; thus, AlN can nucleate on these sites, as shown in Fig. 4(e). Putting simply, AlN nucleation follows the sequence of the N-doped position in graphene from its step edges to centers. Moreover, the 0.07 eV migration barrier enables Al to migrate freely along defect-free graphene. Therefore, AlN nuclei on graphene tend to enlarge rather than dense nucleation sites on bare sapphire; see Fig. 4(f). Finally, the GaN film with a flat morphology and low TDs is realized with the underneath AlN nucleation layer, as shown in Fig. 4(g), which is attributed to the low nucleus density and reduced grain boundaries of GaN.

In summary, this work demonstrated the growth mechanism of GaN quasi-van der Waals epitaxy on *in situ* N-doping in graphene using AlN nuclei by both experiment and the first-principles calculation. Raman and XPS results proved the formation of defects and *in situ* N-doping in graphene during AlN growth in the MOCVD system. The first-principles calculation confirmed that N atoms dope initially at the step edge of graphene and subsequently at its center as time increases, and AlN nuclei followed the same nucleation sequence. Moreover, AlN nuclei on graphene were larger and less dense than those on the sapphire substrate because of the low migration barrier. Thus, the growth mechanism and corresponding growth model of GaN quasi-van der Waals epitaxy on graphene with an AlN nucleation layer were established. This work serves as guidance for quasi-van der Waals epitaxy of high-quality III-nitrides on graphene.

See the supplementary material for (1) the graphene transfer and GaN epitaxy process, (2) SEM images of AlN nucleation in the large-view field, (3) thickness mapping of GaN on graphene, (4) XPS of N1s at different stages of AlN growth, (5) PL spectra of GaN, and (6) detailed first-principles calculation methods.

This work was supported by the National Natural Science Foundation of China (Nos. 61922078, 61725403, 61827813, and 61874118), the National Key R&D Program of China (No. 2017YFB0404103), the Department of Science and Technology of Jilin Province (No. 20180201026GX), the Youth Innovation Promotion Association of the Chinese Academy of Sciences (No. Y201945), The Open Project of State Key Laboratory of Luminescence and Applications (No. E00522NZM100), and the Suzhou Institute of Nano-Tech and Nano-Bionics (No. 20YZ10).

DATA AVAILABILITY

The data that support the findings of this study are available from the corresponding author upon reasonable request.

REFERENCES

[1]D. C. Look and Z. Q. Fang, Appl. Phys. Lett. **79**, 84 (2001).
[2]L. W. Sang, B. Ren, R. Endo, T. Masuda, H. Yasufuku, M. Y. Liao, T. Nabatame, M. Sumiya, and Y. Koide, Appl. Phys. Lett. **115**, 172103 (2019).
[3]T. Sakai, M. Kushimoto, Z. Y. Zhang, N. Sugiyama, L. J. Schowalter, Y. Honda, C. Sasaoka, and H. Amano, Appl. Phys. Lett. **116**, 122101 (2020).
[4]D. B. Chen, Z. K. Liu, J. H. Liang, L. J. Wan, Z. L. Xie, and G. Q. Li, J. Mater. Chem. C **7**, 12075 (2019).
[5]M. Snure, G. Siegel, D. C. Look, and Q. Paduano, J. Cryst. Growth **464**, 168 (2017).
[6]D. B. Li, K. Jiang, X. J. Sun, and C. L. Guo, Adv. Opt. Photonics **10**, 43 (2018).
[7]T. A. Growden, W. D. Zhang, E. R. Brown, D. F. Storm, D. J. Meyer, and P. R. Berger, Light **7**, 17150 (2018).
[8]M. S. Chae, T. H. Lee, K. R. Son, Y. W. Kim, K. S. Hwang, and T. G. Kim, Nanoscale Horiz. **4**, 610 (2019).
[9]Y. Sun, K. Zhou, M. X. Feng, Z. C. Li, Y. Zhou, Q. Sun, J. P. Liu, L. Q. Zhang, D. Y. Li, X. J. Sun, D. B. Li, S. M. Zhang, M. Ikeda, and H. Yang, Light **7**, 13 (2018).
[10]Y. Wu, Z. W. Li, K. W. Ang, Y. P. Jia, Z. M. Shi, Z. Huang, W. J. Yu, X. J. Sun, X. K. Liu, and D. B. Li, Photonics Res. **7**, 1127 (2019).
[11]T. Zimmermann, D. Deen, Y. Cao, J. Simon, P. Fay, D. Jena, and H. G. Xing, IEEE Electron Device Lett. **29**, 661 (2008).
[12]N. Grandjean, J. Massies, I. Grzegory, and S. Porowski, Semicond. Sci. Technol. **16**, 358 (2001).
[13]M. Araki, N. Mochimizo, K. Hoshino, and K. Tadatomo, Jpn. J. Appl. Phys., Part 1 **47**, 119 (2008).
[14]H. L. Chang, Z. L. Chen, W. J. Li, J. C. Yan, R. Hou, S. Y. Yang, Z. Q. Liu, G. D. Yuan, J. X. Wang, J. M. Li, P. Gao, and T. B. Wei, Appl. Phys. Lett. **114**, 091107 (2019).
[15]P. Wang, A. Pandey, J. Gim, W. J. Shin, E. T. Reid, D. A. Laleyan, Y. Sun, D. H. Zhang, Z. Liu, Z. H. Zhong, R. Hovden, and Z. T. Mi, Appl. Phys. Lett. **116**, 171905 (2020).
[16]K. Chung, C. H. Lee, and G. C. Yi, Science **330**, 655 (2010).
[17]Y. Kim, S. S. Cruz, K. Lee, B. O. Alawode, C. Choi, Y. Song, J. M. Johnson, C. Heidelberger, W. Kong, S. Choi, K. Qiao, I. Almansouri, E. A. Fitzgerald, J. Kong, A. M. Kolpak, J. Hwang, and J. Kim, Nature **544**, 340 (2017).
[18]Z. B. Zheng, J. T. Li, T. Ma, H. L. Fang, W. C. Ren, J. Chen, J. C. She, Y. Zhang, F. Liu, H. J. Chen, S. Z. Deng, and N. S. Xu, Light **6**, e17057 (2017).
[19]A. E. Galashev and O. R. Rakhmanova, Phys.-Usp. **57**, 970 (2014).
[20]T. Ohta, A. Bostwick, J. L. McChesney, T. Seyller, K. Horn, and E. Rotenberg, Phys. Rev. Lett. **98**, 206802 (2007).
[21]W. C. Ke, Z. Y. Liang, S. T. Tesfay, C. Y. Chiang, C. Y. Yang, K. J. Chang, and J. C. Lin, Appl. Surf. Sci. **494**, 644 (2019).
[22]A. L. Mulyo, M. K. Rajpalke, H. Kuroe, P. E. Vullum, H. Weman, B. O. Fimland, and K. Kishino, Nanotechnology **30**, 049601 (2019).
[23]S. J. Chae, Y. H. Kim, T. H. Seo, D. L. Duong, S. M. Lee, M. H. Park, E. S. Kim, J. J. Bae, S. Y. Lee, H. Jeong, E. K. Suh, C. W. Yang, M. S. Jeong, and Y. H. Lee, RSC Adv. **5**, 1343 (2015).
[24]T. B. Li, C. Y. Liu, Z. Zhang, B. Yu, H. L. Dong, W. Jia, Z. G. Jia, C. Y. Yu, L. Gan, B. S. Xu, and H. W. Jiang, Nanoscale Res. Lett. **13**, 130 (2018).
[25]Z. L. Chen, Z. Q. Liu, T. B. Wei, S. Y. Yang, Z. P. Dou, Y. Y. Wang, H. N. Ci, H. L. Chang, Y. Qi, J. C. Yan, J. X. Wang, Y. F. Zhang, P. Gao, J. M. Li, and Z. F. Liu, Adv. Mater. **31**, 1807345 (2019).
[26]J. K. Choi, J. H. Huh, S. D. Kim, D. Moon, D. Yoon, K. Joo, J. Kwak, J. H. Chu, S. Y. Kim, K. Park, Y. W. Kim, E. Yoon, H. Cheong, and S. Y. Kwon, Nanotechnology **23**, 435603 (2012).
[27]Y. X. Feng, X. L. Yang, Z. H. Zhang, D. Kang, J. Zhang, K. K. Liu, X. Z. Li, J. F. Shen, F. Liu, T. Wang, P. F. Ji, F. J. Xu, N. Tang, T. J. Yu, X. Q. Wang, D. P. Yu, W. K. Ge, and B. Shen, Adv. Funct. Mater. **29**, 1905056 (2019).
[28]A. L. Mulyo, M. K. Rajpalke, P. E. Vullum, H. Weman, K. Kishino, and B. O. Fimland, Sci. Rep. **10**, 853 (2020).
[29]Z. M. Shi, X. J. Sun, Y. P. Jia, X. K. Liu, S. L. Zhang, Z. B. Qi, and D. B. Li, Sci. China-Phys. Mech. Astron. **62**, 127311 (2019).
[30]L. B. Freund and S. Suresh, *Thin Film Materials-Stress, Defect Formation and Surface Evolution* (Cambridge University Press, 2003).
[31]Y. Chen, Y. Y. Yue, S. R. Wang, N. Zhang, J. Feng, and H. B. Sun, Sol. Energy Mater. Sol. Cells **201**, 110075 (2019).
[32]A. C. Ferrari, J. C. Meyer, V. Scardaci, C. Casiraghi, M. Lazzeri, F. Mauri, S. Piscanec, D. Jiang, K. S. Novoselov, S. Roth, and A. K. Geim, Phys. Rev. Lett. **97**, 187401 (2006).
[33]C. H. Zhang, L. Fu, N. Liu, M. H. Liu, Y. Y. Wang, and Z. F. Liu, Adv. Mater. **23**, 1020 (2011).
[34]Y. C. Lin, C. Y. Lin, and P. W. Chiu, Appl. Phys. Lett. **96**, 133110 (2010).
[35]J. Yan, Y. B. Zhang, P. Kim, and A. Pinczuk, Phys. Rev. Lett. **98**, 166802 (2007).
[36]G. Kresse and D. Joubert, Phys. Rev. B **59**, 1758 (1999).
[37]D. Sheppard, P. Xiao, W. Chemelewski, D. D. Johnson, and G. Henkelman, J. Chem. Phys. **136**, 074103 (2012).